JOURNAL OF MATERIALS SCIENCE 26 (1991) 6383–6390

# Fracture of alumina: an experimental and numerical study

J. LLORCA
*Departamento de Ciencia de Materiales, Universidad Politécnica de Madrid, ETS Ingenieros de Caminos, Ciudad Universitaria. 28040 Madrid, Spain.*

R. W. STEINBRECH
*Institut für Reaktorwerkstoffe. Forschunszentrum Jülich, Postfach 1913. D-5170, Jülich, Germany*

A numerical analysis of the fracture behaviour of alumina has been performed based on experimental crack growth studies. Single-edge notch bend and short-double cantilever beam specimens of diverse grain size alumina were tested under quasi-static growth conditions. Constitutive equations for the alumina were obtained from experimental results and used to carry out finite element analyses. The agreement between numerical and experimental results is very promising, e.g. the influence of grain size on fracture behaviour can be predicted accurately. The underlying toughening mechanisms are discussed.

## 1. Introduction

Ceramic materials exhibit several favourable properties (chemical inertness, high temperature capability, low density, hardness, stiffness and compressive strength) which make them potential products to be employed in many different engineering applications [1]. Their poor fracture resistance and brittle behaviour, that lead to catastrophic failures, have, however, prevented their use on many occasions. Although much research effort has been carried out in recent years in order to gain a better knowledge of the fracture mechanisms in these materials, some questions are still unsolved, even for monolithic ceramics.

At first glance, monolithic ceramics seem ideal materials for application of linear elastic fracture mechanics (LEFM): in general they are brittle and do not experience plastic deformation, at least at room temperature. Today, however, there is strong experimental evidence that the fracture behaviour of ceramics has to be analysed more carefully. Some ceramics show a macroscopic increase in the fracture resistance ($R$) as the crack grows. This *R-curve* is not a unique material property but depends on geometry and testing conditions [2–5]. Experimental crack growth studies of long cracks in alumina have shown that the source of this non-linearity is not located ahead of the crack tip but in the "wake" of the crack. There is compelling evidence of crack surface interaction, e.g. by frictional tractions around bridging grains, which produces a strong toughening effect. Although microcracking or damage in the frontal crack tip zone has been reported recently [6], there is no experimental evidence that such a frontal microcrack zone significantly contributes to an increasing crack resistance [7, 8]. A microcrack zone, once part of the wake, may, however enhance the frictional tractions because of the dilational strains. When the material behind the crack tip is removed, the fracture resistance drops to the initial value in a notched specimen, indicating that wake effects in the rear part of the crack are causing the *R-curve* behaviour [9]. This *wake zone* can reach some millimetres [in length], approximately the same order of magnitude as the crack length, consistent with the strong crack size effects experimentally observed. This kind of behaviour was found to occur in concrete and cementitious composites more than ten years ago and now it is widely accepted that fracture toughness, (e.g. $K_{Ic}$) in the classical sense of LEFM, cannot be used to explain the fracture of these materials [10].

In order to explain these phenomena, various models have been developed [11–14]. All these models can be considered as simplifications of the cohesive crack model (CCM). This model, proposed by Hillerborg *et al.* [15], can be treated as a particular case of the Barenblatt model [16]. The material behaves in a linear elastic manner outside of the crack. The crack is, however, able to transfer stresses in between its surfaces. The cohesive stress $\sigma$ at a given interaction site depends on the crack opening displacement $w$ in that position, according to a strain-softening relationship $\sigma$–$w$ which is a material property. This leads to a linear elasticity problem with non-linear boundary conditions that must be solved by means of numerical methods. In order to simplify the solution, the former quoted models [11–14] make the assumption that the crack faces remain straight during the crack propagation. The accuracy of this hypothesis has not been rigorously proved, although some experimental results support it. Moreover,

0022–2461/91 $03.00 + .12 

additional suppositions are needed about the magnitude of the angle between crack surfaces during crack propagation.

The main disadvantage of the model is that the softening curve $\sigma$–$w$ cannot be measured experimentally because of the strain localization within the crack. Similarly, it is not possible to measure the stress–strain relationship for a metal after necking begins. The softening curve is therefore chosen, in the previously mentioned models, in such a way that it matches the experimental results. Even so, there is no clear evidence of whether or not it is geometry dependent.

The aim of this paper is to study the applicability of the CCM to characterize the fracture behaviour of a monolithic ceramic, such as pure polycrystalline alumina. Both experimental and numerical analyses have been carried out. Experimentally, two different geometries with varying notch depths have been tested. The variables needed to check the model have been measured; fracture energy, fracture resistance, crack length, etc. A special effort has been made to determine the constitutive equation for the cohesive crack from the available experimental data and to minimize the number of adjustable parameters. The strain-softening curve features have been related to the microstructural characteristics and the mechanical properties of the $Al_2O_3$. In the numerical field, a detailed finite element analysis of the geometries tested has been performed. The finite element solution of the displacement field in the cohesive crack is more accurate than the one assumed by the simplified models previously mentioned. When these precautions are taken, it is expected that it will become clear whether the CCM is able to explain the fracture behaviour of polycrystalline alumina or the agreement between numerical and experimental results, reported in other investigations, is a result of the possibility of choosing freely some of the parameters of the model. The influence of the grain size on the fracture resistance and brittleness is also studied.

## 2. Experimental procedure

Various high purity aluminas were tested. All of them were processed from the same starting powder (CT 8000, Alcoa, Frankfurt a. M., FRG). Samples were cold isostatically densified and sintered in air at 1700 °C using different holding times to obtain average grain sizes of 4, 9 and 16 μm.

Single-edge notched bend (SENB) and short double cantilever beam specimens (s-DCB) were machined from these batches (dimensions sketched in Fig. 1). All specimens were fractured under conditions of slow, quasi-static crack growth, from a starter notch of depth $a_0$. Load ($F$), load–point displacement ($\delta$), crack length ($a$) and crack opening displacement at the initial notch CTOD were recorded during tests (the last two parameters with a travelling microscope) and the crack resistance was evaluated applying a linear elastic compliance method.

SENB specimens, from the 16 μm grain size batch, with four different initial notch lengths were tested

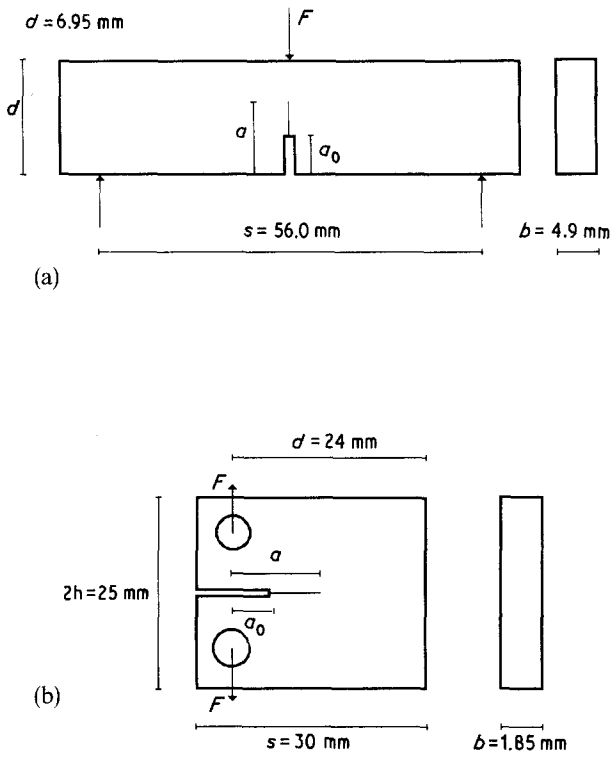


*Figure 1* Geometry and dimensions of the specimens. (a) SENB, (b) s-DCB

($a_0/d = 0.22$, 0.40, 0.60 and 0.75). Only one notch length was used with s-DCB specimens ($a_0/d = 0.67$). Two or three tests were carried out with each geometry in order to check repeatability. In addition, SENB specimens from the 4 and 9 μm grain size batches, with an initial notch length $a_0/d = 0.60$, were tested to study grain size effects on fracture and brittleness. Tests results and discussion are presented in the next sections.

## 3. Cohesive Crack Model

### 3.1. Hypotheses

The CCM assumes that the material behaves in a linear and isotropic manner, both in tension and compression, when stresses are below the tensile strength $\sigma_t$. The material is then characterized by means of Young's modulus $E$ and Poisson's modulus $\nu$, without any reference to anelastic or time dependent phenomena. Values for these parameters have been chosen from literature [17], as $E = 360$ GPa and $\nu = 0.23$.

When the stress overcomes $\sigma_t$ in one point of the material, a cohesive crack perpendicular to the maximum tensile stress appears in this zone. Deformation is localized within the crack and the relation between crack opening displacement $w$ and transferred stress $\sigma$ is given by the softening curve (Fig. 2), a material property according to the CCM. The softening curve can be chosen rather arbitrarily but must always fit some restraints. Firstly, when $w = 0$, the stress transferred through the crack has to be equal to $\sigma_t$. Secondly, there is critical value of $w$, named $w_c$, defined such that if $w \geqslant w_c$ then $\sigma = 0$. Finally, the area under the softening curve is the fracture energy $G_F$;

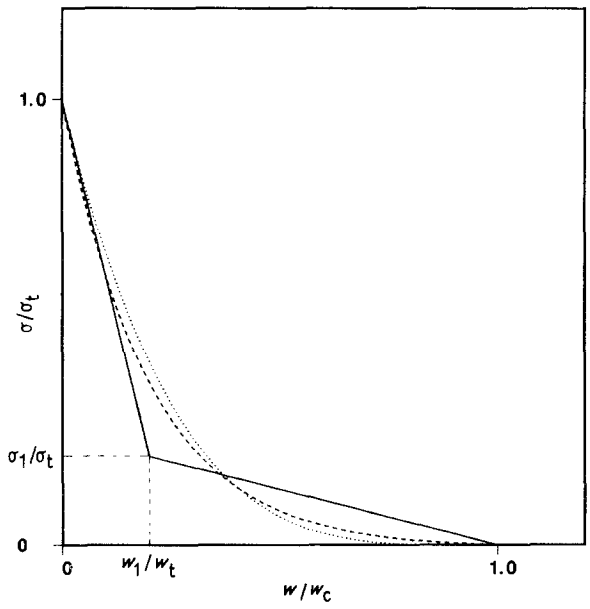


*Figure 2* Strain softening curves. (——bilinear, – – –exponential, . . . . . power law)

that is the energy needed by unit area to create a new separated surface.

The material will develop an interaction zone, where cohesive stresses are acting, in response to an external load. The CCM assumes that there is not stress singularity at the tip of the crack because the stress at that point is $\sigma_t$. The length of the interaction zone and the intensity of the cohesive forces depend on the strain-softening curve and on the external load. Both can be evaluated taking into account that the stress intensity factor due to cohesive forces must be equal to the one induced by external forces. This fact implies solving a non-linear problem because the displacements behind the crack tip are a function of both external and cohesive forces. When the cohesive forces can no longer equilibrate the stress intensity factor, the crack tip will propagate a definitive length and new bridging forces will be produced behind it.

No material can withstand an infinite stress. In metallic alloys, plastic deformation occurs around the crack tip, blunting the crack and avoiding stress singularity. When dislocation plasticity is not very likely (as happens in brittle materials such as ceramics, concrete, rocks, etc.), a different mechanism must appear in order to shield the crack against infinite stresses. In MgO partially stabilized zirconia, which is a particularly tough ceramic, tetragonal precipitates of zirconia, ahead of the crack tip, undergo a martensitic-type transformation to the larger-volume monoclinic symmetry when external stress is applied. This mechanically induced transformation produces a volumetric strain and shear distortion. This, in turn, causes energy to be dissipated and the stress concentration to be smoothed out. Another mechanism of relaxation of the high stress gradients ahead the crack tip is microcracking. Extensive microcracking is very often found in fracture tests of ceramics and ceramic composites at elevated temperatures. The microcracks, that are developed along grain boundaries and interfaces, reduce the elastic modulus of the material and the stresses ahead of the crack tip. Finally, crack tip shielding in brittle materials can be achieved by the development of cohesive forces behind the crack tip that equilibrate the external crack driving force.

The use of the CCM to study the fracture behaviour of one particular material is justified when the main toughening mechanism is due to the development of cohesive forces. In polycrystalline alumina neither dislocation plasticity nor transformation toughening take place and, thus, microcracking and interactions in the wake of the crack are the main candidates to account for crack growth resistance in $Al_2O_3$. Microcracking of $Al_2O_3$ at room temperature has been reported recently [4] but other studies have not found it [6, 7], and to date there is no evidence that the microcrack zone contribution dominates the experimentally observed crack growth resistance.

According to the hypotheses of the CCM, when a specimen of a cohesive material is loaded up to final failure, the work of the external forces must be equal to $G_F$ times the cracked area because all of the energy supplied to the specimen is employed in creating new free surfaces. In other words, the fracture energy experimentally measured as the ratio between the external work and the surface crack area, must be constant and independent of geometry and loading conditions. $G_F$ values are shown in Table I for the four different SENB and the s-DCB specimens of 16 μm average grain size $Al_2O_3$ tested. Fracture energy is fairly constant with a mean value of 76 $N m^{-1}$. These results indicate that energy dissipation due to microcracking in front of the crack tip is not a relevant quantity. The damage induced due to microcracking increases with maximum load, which depends on geometry, initial notch length and size. If this mechanism was active, the bigger the specimens, the more energy per unit area would be used to break them. It may thus be concluded that the cohesive forces developed behind the crack tip, due to grain bridging and interlocking, are the most important toughening mechanism in polycrystalline alumina. Then, the CCM seems to be appropriate to model its fracture behaviour.

## 3.2. Determination of the softening curve for alumina

As was pointed out before, the fracture behaviour is determined by the $\sigma$–$w$ relationship. The origin of this behaviour is well documented from the experimental point of view: microscopic *in situ* observations of the crack path have shown the existence of crack surface interactions [7, 18], crack bridging due to serrated grains [18] and unbroken ligaments [19]. There is, however, presently no experiment known to the authors which measures directly the amount of

TABLE I Experimentally measured fracture energy for $Al_2O_3$

| Specimen type | SENB | SENB | SENB | SENB | s-DCB |
|---|---|---|---|---|---|
| $a_0/d$ | 0.22 | 0.40 | 0.60 | 0.75 | 0.67 |
| $G_F$($N m^{-1}$) | 76.8 | 72.2 | 80.2 | 71.4 | 78.1 |

stresses transferred between the crack faces and therefore indirect procedures must be employed in order to evaluate the softening curve shape.

The tensile strength $\sigma_t$ was chosen equal to 200 MPa, in accordance with the values reported in the literature [17]. In addition, Steinbrech *et al.* [14] have recently measured the critical value of the crack opening displacement $w_c$ for different grain size polycrystalline aluminas and found that it is equal to one quarter of the mean grain size. They rationalize this experimental result quite simply: on average an individual grain should be removable from the opposite crack surface if it is implanted there with a depth between zero and one half of its diameter. Otherwise it is extracted from the actual surface; thus, on average, one quarter of the diameter defines separation.

Different softening curve shapes have been proposed successfully for various materials: bilinear and exponential softening curves for concrete and lightweight concrete [20, 21]; power-law softening for cementitious composites and monolithic ceramics [11, 14, 22]. Recently, the CCM has been used to evaluate the fracture behaviour of fibre-reinforced C–SiC ceramic matrix composite [23]. The analytical expression of the softening curve was theoretically determined from the mechanical properties of the matrix, fibres and interfaces, according to the studies of Thouless and Evans [24]. It has been found that the stress transferred through the crack increases at the beginning with the displacement $w$ due to the bridging effect of the fibres. After reaching a maximum, the softening curve shows a descent in the cohesive stresses and the shape of the curve is almost bilinear. The two branches of the bilinear softening curve respond to different mechanisms of energy dissipation: the first takes into account the bridging effect of the fibres just behind the crack tip and the second is related to decohesion and pull-out between fibres and matrix.

When the values of $\sigma_t$, $w_c$, and $G_F$ are fixed, the different types of softening curves look very much alike (Fig. 2) and the finite element analyses further show that similar results are obtained [13]. Thus, we have chosen a bilinear softening curve, given by

$$\sigma = \sigma_t - \frac{\sigma_t - \sigma_1}{w_1} w \qquad \text{if } 0 \leqslant w \leqslant w_1 \quad (1a)$$

$$\sigma = \sigma_1 - \frac{\sigma_1}{w_c - w_1}(w - w_1) \qquad \text{if } w_1 \leqslant w \leqslant w_c \quad (1b)$$

$$\sigma = 0 \qquad \text{if } w \geqslant w_c \quad (1c)$$

where $w_1$ and $\sigma_1$ are the displacement and the stress at the knee, respectively. If we consider that

$$G_F = \frac{\sigma_t w_1 + \sigma_1 w_c}{2} \quad (2)$$

there is only one degree of freedom that we can use to fit experimental and numerical results.

## 3.3. Numerical procedure

The numerical technique of the influence matrices has been used to solve this non-linear problem [20]. The outline of this procedure is: let us assume we have a linear elastic solid in which a cohesive crack has been propagated in mode I from an initial notch (located in the node $n_0$) up to node $k$ due to an external load $F$ (Fig. 3). The cohesive forces $P_j$ applied in the nodes and the crack opening displacements $w_i$ are related according to the expression

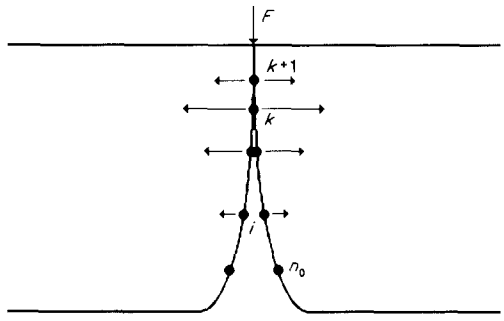


*Figure 3* Numerical analysis of a cohesive crack. Notation

$$w_i = K_{ij} P_j + C_i F, \; i = n_0, k \quad (3)$$

where $K$ and $C$ are influence matrices. The element $K_{ij}$ represents the crack opening displacement in the node $i$ when a unit force is applied in the node $j$. In the same way, the element $C_i$ is the crack opening displacement produced in the node $i$ when a unit external force is applied. The relationship between cohesive forces and crack openings is given by

$$P_j = \begin{cases} \Delta a b \sigma(w_j)/2 & \text{if } j = n_0 \\ \Delta a b \sigma(w_j) & \text{if } j = n_0 + 1, \; k - 1 \\ \Delta a b \sigma_t & \text{if } j = k \end{cases} \quad (4)$$

where $\sigma(w)$ is the softening function, $b$ the thickness of the specimen and $\Delta a$ the distance between adjacent nodes. The factor 2 dividing the load in the node $n_0$ is due to the fact that only one half of the crack around the notch is within the cohesive zone. If we add the condition that $w_k = 0$ to Equations 3 and 4, we have a non-linear system of equations that we can solve using the Newton method. The results of the analysis are the stresses and displacements on the cohesive crack and the external load. We can now assume that the crack has propagated one element (up to the node $k + 1$) and repeat the whole procedure. The main advantage of this procedure is that the number of active degrees of freedom is reduced to those on the cohesive zone and the solution of these small non-linear systems of equations is very fast. The effort to evaluate the influence matrices has to be done only once for each geometry.

After each crack increment, we can evaluate the displacements on the crack by means of Equation 3 and the displacement of the loading point $\delta$ is given by

$$\delta = D_j P_j + D_F F \quad (5)$$

where $D$ is a new influence matrix. $D_j$ is the displacement of the loading point when a unit force is applied on the node $j$. $D_F$ is the displacement of the loading point when a unit force is acting on this point.

When both the external load and the crack length are known, the calculation of the fracture resistance

TABLE II Softening curve parameters for $Al_2O_3$

| Grain size (μm) | $\sigma_t$ (MPa) | $w_c$ (μm) | $G_F$ (N m$^{-1}$) | $G_{F1}$ (N m$^{-1}$) | $G_{F2}$ (N m$^{-1}$) | $w_1$ (μm) | $\sigma_1$ (MPa) |
|---|---|---|---|---|---|---|---|
| 16 | 200 | 4.00 | 76.1 | 43.6 | 32.5 | 0.4 | 18.06 |
| 9 | 200 | 2.25 | 60.3 | 43.6 | 16.7 | 0.4 | 18.06 |
| 4 | 200 | 1.00 | 49.0 | 43.6 | 5.4 | 0.4 | 18.06 |

$R$ is straightforward, according to the expression,

$$R = \frac{K_R^2}{E} \tag{6}$$

where $K_R$ is the applied stress intensity factor. $K_R$ can also be calculated by summing up the stress intensity factors due to the cohesive forces. When a stress $\sigma(x)$ is applied on a crack of length $a$, as depicted in Fig. 4, the stress intensity factor is,

$$dK_\sigma(a, x) = \frac{2\sigma(x)}{(\pi a)^{1/2}} H\left[\frac{a}{d}, \frac{x}{a}\right] dx \tag{7}$$

where the non-dimensional function $H(a/d, x/a)$ depends on the geometry and, for a beam of infinite length, can be found in the literature [24]. The crack growth resistance due to all the cohesive forces is thus given by

$$K_R(a) = \int_{a_0}^{a} \frac{2\sigma(x)}{(\pi a)^{1/2}} H\left[\frac{a}{d}, \frac{x}{a}\right] dx \tag{8}$$

Expression 8 shows that the crack growth resistance is a complex function of the softening curve and the geometry. In the asymptotic limit, when the length of the cohesive zone is very small compared with the crack length and the crack is embedded in an infinite solid, the fracture resistance $R^\infty$ is equal to the fracture energy $G_F$. When these limit conditions do not occur, however, the fracture resistance curve will depend strongly at the beginning on $\sigma_t$ and the slope of the softening curve. As the wake interaction zone develops, the whole shape of the softening curve, and not only the value of $G_F$, influences the crack growth resistance curve.

Finally, the numerical analyses carried out show that the length of the wake interaction zone shrinks when the crack tip is nearing the back face of the specimen. In that situation, the effect of $\sigma_t$ and the shape of the softening curve on the fracture resistance are less important and $R$ is mainly a function of the total fracture energy $G_F$ and the geometry.

The influence matrices $K$, $C$, $D$ and the coefficient $D_F$ for the SENB geometry were obtained using the finite element method. The mesh used had one hundred elements on the crack, in order to capture the high stress gradients that are found around the cohesive crack. As the material outside of the crack is linear elastic, the influence matrix coefficients can be used for materials with different elastic properties through simply multiplying by the ratios of the elastic constants.

## 4. Results and discussion

### 4.1. Fracture resistance curve

Experimental results of crack growth resistance against crack length are shown in Fig. 5 for SENB specimens of the material with grain size equal to 16 μm. Results of different tests for each initial notch length are very similar but strong effects of specimen geometry can be noticed on crack resistance curves. The solid lines in the same figure are the results obtained by applying the CCM. The material properties used are listed in Table II. As was mentioned before, only one parameter ($w_1$) was chosen freely in order to match experimental and numerical results. As can be seen, there is a very good agreement between both. In addition to this, experimental and numerical results of the load ($F$) against displacement ($\delta$) curves have been plotted in Fig. 6a to d for the four SENB geometries. Again, the agreement is good not only in the magnitude of the maximum load but also in the tail of the curves. The value of the flexure elastic modulus used to evaluate these curves was 252 GPa and it was

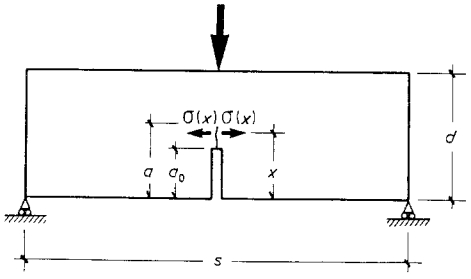


*Figure 4* Single-edge notched bend specimen notation.

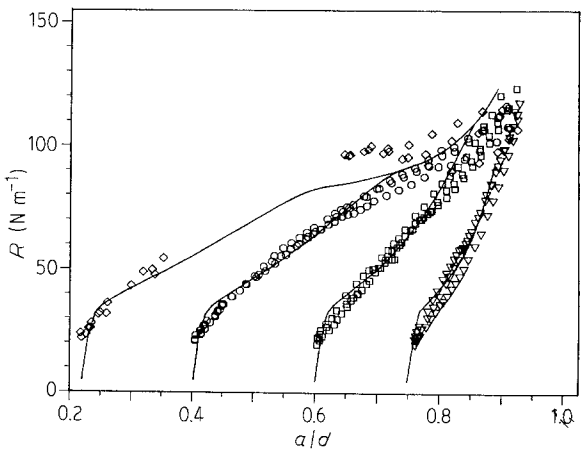


*Figure 5* Crack growth resistance curves for coarse grained $Al_2O_3$ (grain size 16 μm). SENB specimens. Solid lines show the numerical results.

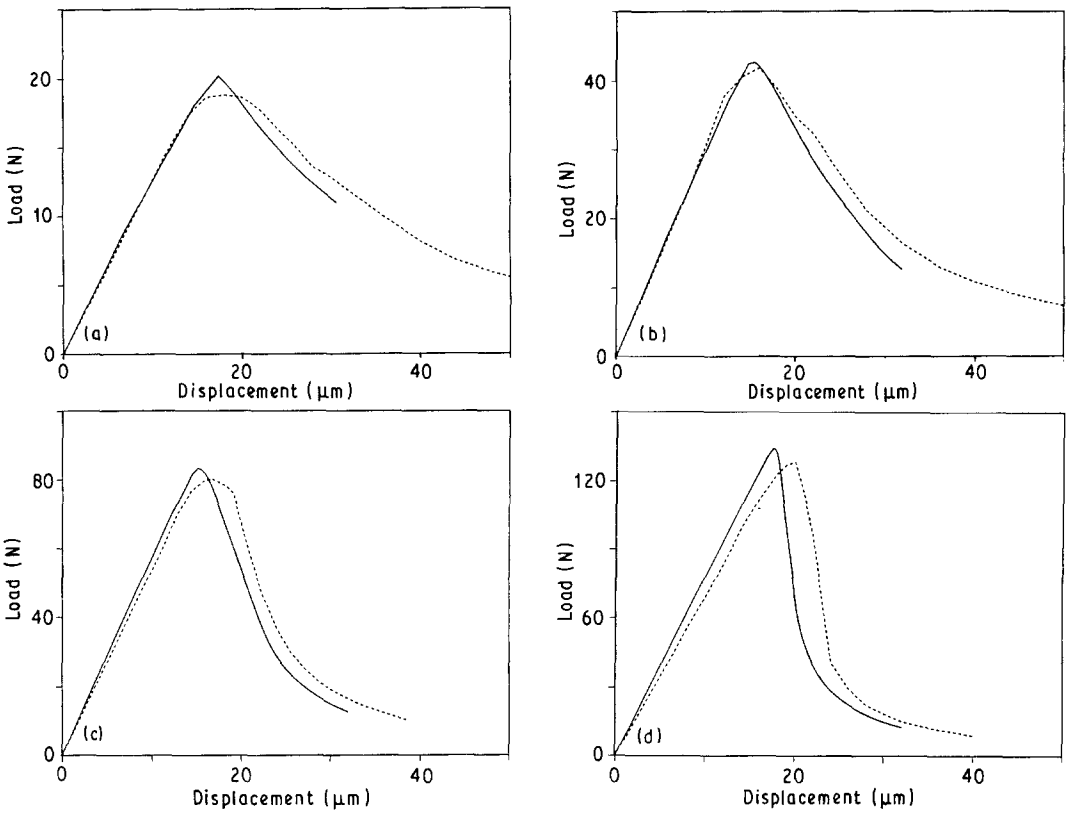


*Figure 6* Experimental (dashed line) and calculated (solid line) load–displacement curves for $Al_2O_3$. Grain size 16 μm. (a) $a_0/d = 0.75$, (b) $a_0/d = 0.60$, (c) $a_0/d = 0.40$, (d) $a_0/d = 0.22$.

determined from the experimentally measured initial compliances. Fig. 7 shows both numerical and experimental results of CTOD against crack length.

These results support the assumption that fracture behaviour of $Al_2O_3$ at room temperature can be correctly modelled by means of the CCM, especially if the experimental evidence that has been discussed in previous sections is taken into account. Moreover, through the shape of $R$-curves it is possible to obtain a better understanding of fracture processes in these materials. As can be seen in Fig. 5, the $R$-curve rises almost vertically from the beginning of the test, up to an initial value close to 35 $N m^{-1}$. A sharp change in the slope from this point takes place, and the $R$-curve continues growing with a slope that seems to be related to the initial notch length. Finally, all the curves merge when the crack has propagated to 90% of the beam depth. The fast initial growth of the fracture resistance is due to the high cohesive stresses that are developed just behind the crack tip. The value attained after this initial growth does not depend on the geometry (because the size of the wake zone is small compared with notch length and the specimen's dimensions) and it is related to the fracture energy $G_{F1}$ (see Table II) which is defined as

$$G_{F1} = \int_0^{w_1} \sigma(w)\,dw = \frac{\sigma_t + \sigma_1}{2} w_1 \qquad (9)$$

as opposed to $G_{F2}(G_{F2} = G_F - G_{F1})$. Crack bridging due to serrated grains and unbroken ligaments [19] or non-uniform through-thickness crack propagation and the presence of localized fields of residual stresses can be the physical mechanisms responsible for such behaviour. All of them have in common that they are able to develop high cohesive stresses when small displacements are involved. The crack opening displacement profiles (see Fig. 8) show that this zone, characterized for COD values under 0.4 μm, is quickly developed when the crack begins to propagate. The size of this zone is always very small and, therefore, the amount of energy dissipated can be considered a specific property of the material that remains constant in spite of other microstructural parameters such as grain size.

After this initial stage, the fracture process zone is fully developed behind the crack tip. Its length (COD under 4 μm in Fig. 8) can extend some millimetres, according to experimental observations in $Al_2O_3$ [7, 8]. The $R$-curves for different initial notch lengths meet when the crack tip is nearing the back face of the specimen. In this situation, the fracture process zone

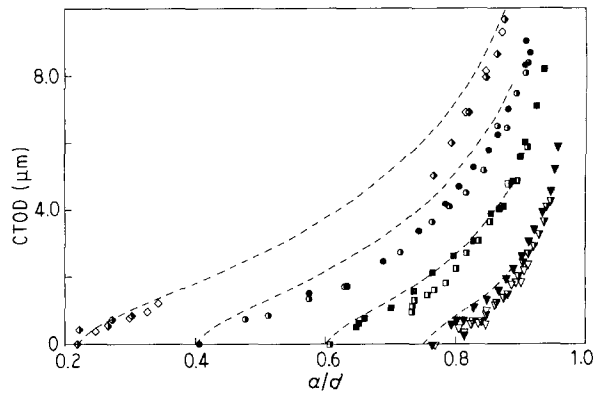


*Figure 7* Displacements at the initial notch tip for coarse grained alumina. SENB geometry. Broken lines show the numerical results.

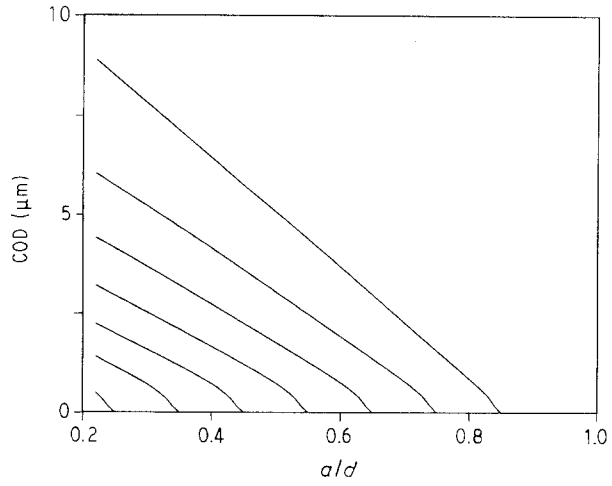


*Figure 8* Evolution of crack profile with crack length.

shrinks and its length is the same for all the specimens. The fracture resistance of the specimens at this point depends only on the total fracture energy $G_F$ because the shape of the softening curve is the same for all.

A brief comment can be made at this point concerning the accuracy of the simplified models developed to apply the CCM to ceramic materials [11–14]. The main assumption of these models (crack surfaces remain straight during crack growth) can be verified with the crack displacement profiles in Fig. 8. The general behaviour is well predicted but we must be aware that small changes in COD near the crack tip lead to relatively large changes in crack growth resistance. This may explain why the softening curve parameters differ among the various models in order to explain experimental results. These differences reflect the degree of accuracy of each model and not diverse constitutive equations.

## 4.2. Influence of grain size

*R*-curves can be seen in Fig. 9 for $Al_2O_3$ with various grain sizes. The specimens' geometry was SENB with an initial notch length $a_0 = 0.6d$. Softening curve parameters, listed in Table II, have been chosen in harmony with the criteria mentioned before. The parameters $\sigma_1$, $w_1$, and $\sigma_1$ are not grain size dependent and $w_c$ is equal to one quarter of the grain size. The agreement between numerical and experimental results is good and the *R*-curve shows the features mentioned in the preceding paragraph. As the softening curve is the same for the three materials at the beginning ($w < w_1$), they exhibit identical initial slopes of the fracture resistance curve. When $w$ reaches $w_1$ at the notch, the differences in the softening curve lead to changes in the *R*-curve for the three $Al_2O_3$. The results of the finite element analyses show that, right after this point is attained, the displacements in the wake of the crack are smaller for the fine grained alumina (the material with lower $w_c$ and $G_{F2}$) and the cohesive stresses are larger, leading to a slightly larger crack growth resistance value when compared with the coarser grained $Al_2O_3$. As the maximum load is attained for that value of the crack growth resistance, it turns out that the load bearing capacity of the fine grain alumina is larger than the one shown by the coarser grain materials (Fig. 10). It is also worthwhile to note that the same behaviour can be found in the experimental results plotted in Fig. 9, where, the lower the grain size, the larger the initial value of the crack growth resistance.

The smaller the grain size, the lower the amount of energy that is dissipated due to friction among crack surfaces and grain interlocking. These features are reflected in the model through the $G_{F2}$ value which diminishes with grain size (see Table II). While, for the coarse grained alumina, the amount of energy dissipated just behind the crack tip is roughly the same as that spent in the wake of the crack, the situation changes completely for the fine grained material, where a four-to-one ratio between them can be found. This leads to a more brittle behaviour with finer grain sizes, as can be seen from the load–displacement curves plotted in Fig. 10. This behaviour is also shown in Fig. 9. The $Al_2O_3$ with coarse grain size exhibits a steadly rising *R*-curve, which is caused by the development of the wake interaction zone as the crack grows. On the contrary, the wake interaction zone for

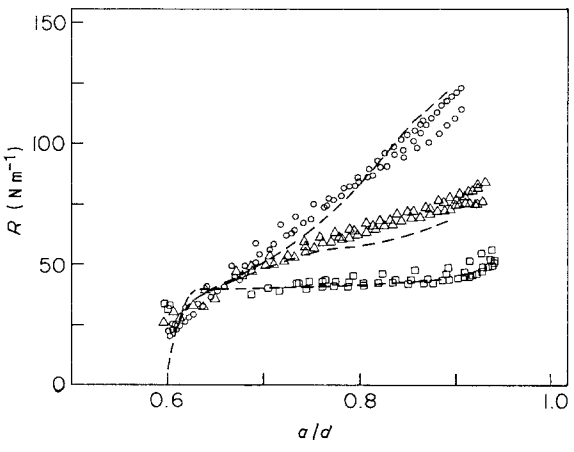


*Figure 9* Crack growth resistance curves for $Al_2O_3$ with various grain sizes (○ 16 μm, △ 9 μm, □ 4 μm). Broken lines show the numerical results.

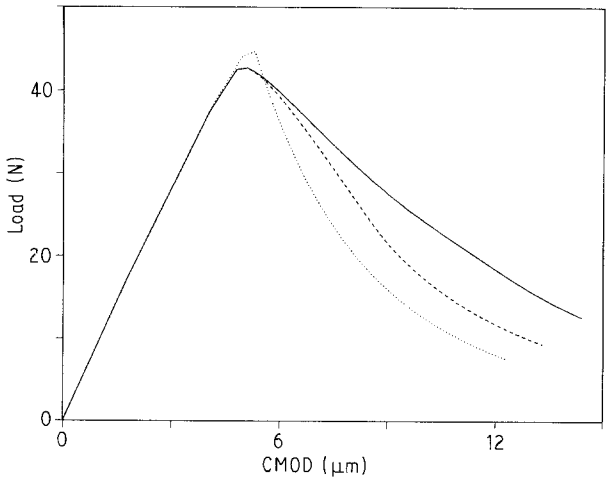


*Figure 10* Calculated load–CMOD curves for $Al_2O_3$ with different grain sizes (—— 16 μm, – – – 9 μm, . . . . . 4 μm). SENB specimens. $a_0/d = 0.6$

the fine grained alumina is fully developed very soon and the material shows a flat crack growth resistance curve. Only when the crack reaches the back face of the specimen is there an increase in the $R$-curve due to the effect of the geometry.

## 5. Conclusions

An experimental and numerical study has been performed to evaluate the ability of the cohesive crack model (CCM) to model the fracture behaviour of polycrystalline alumina. Experimental results show that the fracture energy reaches a value of 76 $N m^{-1}$ for coarse grained alumina and does not depend on geometry or on testing conditions.

A finite element analysis of SENB specimens was performed. Special care was taken in choosing the parameters of the softening curve by means of experimental results. The agreement between numerical and experimental results is very encouraging. It was demonstrated that the influence of geometry and grain size on fracture behaviour of $Al_2O_3$ is accurately predicted by the CCM. The shape of the softening curve seems to find two diverse mechanisms of toughening, both acting in the wake of the crack. The first one, concentrated 100 or 200 μm just behind the crack tip, is able to develop high cohesive stresses and is responsible for the maximum load these materials can bear. The second one is spread out up to some millimetres in the wake of the crack and controls the brittleness of the behaviour in the tail of the load–displacement curves.


## Acknowledgements

The authors are indebted to M. Elices and the members of Cohesive Fracture group (Department of Materials Science, Polytechnic University of Madrid) for the help provided during the development of the numerical technique. The authors also wish to thank R. Dickerson for critically reading the manuscript. The experimental part of this work was financially supported by the German Research Association.


## References


1. J. B. WACHTMAN, (Ed.), "Structural Ceramics" (Academic Press, London, 1989).
2. R. W. STEINBRECH, R. KNEHANS and W. SCHAARWÄCHTER, *J. Mater. Sci.* **18** (1983) 265.
3. F. DEUERLER, R. KNEHANS and R. W. STEINBRECH, *Sci. Ceram.* **13** (1986).
4. *Idem., J. Physique* (1986) C1-617.
5. E. INGHELS, A. H. HEUER and R. W. STEINBRECH, *J. Amer. Ceram. Soc.* **73** (1990) 2023.
6. E. BABILON, K. K. O. BÄR, G. KLEIST and H. NICKEL, in "Euro-Ceramics," edited by G. de With et al. (Elsevier Applied Science, 1989) p. 3.247.
7. P. L. SWANSON, C. J. FAIRBANKS, B. R. LAWN, Y. W. MAI and B. J. HOCKEY, *J. Amer. Ceram. Soc.* **70** (1987) 279.
8. J. A. SALEM, J. L. SHANNON, Jr. and R. C. BRADT *ibid.* **72** (1989) 20.
9. R. KNEHANS and R. W. STEINBRECH, *J. Mater. Sci. Lett.* **1** (1982) 327.
10. F. H. WITTMANN, (Ed.), "Fracture Toughness and Fracture Energy of Concrete" (Elsevier., Amsterdam, 1986).
11. Y. W. MAI and B. R. LAWN, *J. Amer. Ceram. Soc.* **70** (1987) 289.
12. C.-H. HSUEH and P. F. BECHER, *ibid.* **71** (1988) C-234.
13. J. LLORCA and M. ELICES, *Cement Concrete Res.* **20** (1990) 92.
14. R. W. STEINBRECH, A. REICHL and W. SCHAARWÄCHTER, *J. Amer. Ceram. Soc.* **73** (1990) 2009.
15. A. HILLERBORG, M. MODEER and P. E. PETERSSON, *Cement Concrete Res.* **6** (1976) 773.
16. G.I. BARENBLATT, *Adv. Appl. Mech.* **7** (1962) 55.
17. ASM, Guide to Engineering Materials **1** (1986) 64.
18. A. REICHL and R. W. STEINBRECH, *J. Amer. Ceram. Soc.* **71** (1988) C-299.
19. M. V. SWAIN, *J. Mater. Sci. Lett.* **5** (1986) 1313.
20. P. E. PETERSSON, Report TVBM-1006. Division of Building Materials. Lund Inst. Tech., Sweden. (1981).
21. H. A. W. CORNELISSEN, D. A. HORDIJK and H. W. REINHARDT, *Heron* **31** (1986) 45.
22. R. M. L. FOOTE, Y. W. MAI and B. COTTERELL, *J. Mech. Phys. Solids* **34** (1986) 593.
23. J. LLORCA and M. ELICES, *Acta Metall. Mater.* **38** (1990) 2485.
24. M. D. THOULESS and A. G. EVANS, *Acta Metall.* **36** (1988) 517.
25. H. TADA, P. PARIS and G. IRWIN, "The Stress Analysis of Cracks Handbook", Del Research Corporation. (1985).



*Received 19 June*
*and accepted 26 June 1990*